Carbon 184 (2021) 146–155

Contents lists available at ScienceDirect

Carbon

journal homepage: www.elsevier.com/locate/carbon

Research Article

Tensile mechanical characteristics of ultra-thin carbon sulfur nanothreads in orientational order

Yuequn Fu [a], Jianyang Wu [a, b, *], Senbo Xiao [a], Siqi Liu [a], Zhiliang Zhang [a], Jianying He [a, **]

[a] NTNU Nanomechanical Lab, Department of Structural Engineering, Norwegian University of Science and Technology (NTNU), Trondheim, 7491, Norway
[b] Department of Physics, Research Institute for Biomimetics and Soft Matter, Jiujiang Research Institute and Fujian Provincial Key Laboratory for Soft Functional Materials Research, Xiamen University, Xiamen, 361005, PR China

ARTICLE INFO

Article history:
Received 21 April 2021
Received in revised form
5 July 2021
Accepted 3 August 2021
Available online 12 August 2021

Keywords:
Carbon nanothreads
Carbon sulfur nanothreads
Mechanical properties
Deformation mechanism

ABSTRACT

Carbon sulfur nanothreads (CSNTs) mainly composed of two chiral long alkane chains have been recently fabricated from thiophene by a pressure-induced phase transition in low-temperature, but their mechanical properties remain unexplored. Here, the critical roles of morphology and temperature on the tensile characteristics of CSNTs are for the first time examined using molecular dynamic simulations with a first-principles-based ReaxFF forcefield. It is revealed that CSNTs exhibit high tensile Young's modulus, high tensile strength and excellent ductility, and their tensile properties are morphology and temperature dependent. Morphologically, atomic arrangement with various configurations makes every CSNTs possess unique mechanical properties. Thermally, as temperature varies from 1 to 1500 K, CSNTs become mechanically weakened. In comparison with conventional diamond nanothreads (DNTs) and carbon nitride nanothreads (CNNTs), CSNTs show distinct axial elongation mechanisms, with relatively insignificant changes in chemical bond orders and bond length in the skeleton prior to the final rupture. Instead, the stretching of bond angle and dihedral angle mainly contribute to the global axial elongation, while the torsional deformation is limited due to their perfect global symmetry in the configuration. This study provides fundamental insights into the mechanics of ultra-thin CSNT structures.

1. Introduction

Diamond nanothreads (DNTs), as sp^3-bonded one-dimensional (1D) carbon crystalline nanomaterial, show excellent properties that appeal abundance of interests of scientists for the last decades [1–3]. Different from sp^2-bonded carbon nanotubes (CNTs), DNTs formed by the gradual room-temperature compression and decompression of benzene [4] or small-molecule heteroaromatic molecules (such as thiophene [5] and pyridine [6]), which is structurally characterized by extreme-thin sp^3-bonded carbon skeleton framework in a diamond-like tetrahedral core shape [7]. Their fully saturated surface of the carbon-carbon cage can retain single-crystal or one-thread morphology that enables them to be equipped with global subnanometer size along the axis. A nanothread offers a perfect nanomaterial to be a combination of monocrystalline rigidity and unshackled polymer consist of aromatic monomers. Experimental results also observed bends and defects in the nanothreads crystals, with most sp^3-bonded and less sp^2-bonded carbon atoms [8]. There are both packing registry and disregistry in nanothreads. Such a structure makes them one of the subtle artificialities capable of successive periodic and orientational order following its longitudinal direction [5]. It allows this kind of nanothread to exhibit anisotropic property and chemically versatile. These unique features give the promise of their outstanding performances of mechanical [9,10], thermal [11], and electrical [12] properties. It is suggested that they can be applied extensively in artificial muscles [13], soft robotics [14], flexible electronics [15], energy storage materials [16], and many other fields [17,18].

Although there are experimental studies [4–6,19–21] of DNTs focusing on synthesis and characterization of them, their mechanical properties are still experimentally challenging to evaluate due to the extreme-thin structure of DNTs. Thus, the efforts of a series of first-principle calculations [22–24] and molecular dynamics (MD) simulations [2,9,10,25] have contributed to the exploration and investigation of the mechanical properties of DNTs.

* Corresponding author. NTNU Nanomechanical Lab, Department of Structural Engineering, Norwegian University of Science and Technology (NTNU), Trondheim, 7491, Norway.
** Corresponding author.
E-mail addresses: jianyang@xmu.edu.cn (J. Wu), jianying.he@ntnu.no (J. He).

https://doi.org/10.1016/j.carbon.2021.08.006

In general, DNTs are mechanically robust and brittle, while other DNTs with defects [2] or specific structure [9] possess structural-dependent ductile even super-ductile properties. There have been many studies indicating that the mechanical properties of DNTs are highly relevant with both their inherent structure (heteroatoms, molecular morphology, the way of sp^2-or sp^3-hybridization of carbon atoms, functional group, defects and so on) and ambient temperature. For carbon nitride nanothreads by pyridine-driven [9], the nitride atoms were arranged in the skeleton structure of DNTs, resulting in an extremely ductile structure with the stretching limit of 190%, and it was predicted to be applied to the fields of robust sensor, materials with ultra-low temperature resistance, and high-density mechanical energy storage. A recent study using ReaxFF-based MD simulations [10] indicated that the DNTs with classical linear configuration performed higher tensile stiffness of 360–730 GPa than the one with intriguing helical configuration (tensile stiffness of 75–375 GPa). Based on an AIREBO-based MD simulation [26], increasing the number of Stone-Wales (SW) defects can obtain a transition from brittle to ductile performance, and the axial stiffnesses of 700–950 GPa were predicted during the tensile test. A study by using density functional theory [27] approved that the functional groups connecting to the carbon skeleton of DNTs have a negligible influence on their mechanical properties. Besides, according to many previous studies [10,28,29], it can be summarized that temperature plays a determinant role in the mechanical properties of DNTs.

As a finding of a new kind of DNTs, a recent study gives evidence of carbon sulfur nanothreads (CSNTs) derived from five-membered thiophene [5]. Unlike the previous benzene- or pyridine-derived nanothreads, this is a recoverable polymeric product with monoclinic order. Such low symmetry results likely from a crystalline packing with uniformly anisotropic cross-sections. It has a potential application to take higher degrees of synthetic control of carbon nanothreads reaction outcomes, as well as prospective investigations to the characterization of symmetry-dependent properties such as piezoelectricity and nonlinear optical effects. Similarly, the furan-based nanothreads have been synthesized through pressure-induced, which also can be considered as an extension of the synthesis of nanothreads derived from five-membered aromatic molecules[30]. Here, this work focused on the CSNTs. Furthermore, carbon nanothreads attract lots of interest from researchers and scientists, mainly by their excellent mechanical properties (lightweight and high performance). Unfortunately, up to the present, there is no effective experimental method and technique to evaluate their mechanical properties, not to mention the mechanism of high mechanical performance, due to the ultra-tiny structure of CSNTs. So there still are many mechanical behaviors that still are not expatiated.

Herein, this work aims at exploring the mechanical performance of CSNTs by MD simulations. In the field of nanothreads, thiophene is the first time to be used to form nanothreads, forming ultra-thin carbon-skeleton organic materials. Although the sulfur atoms are not in the nanothreads' skeleton, it will be meaningful to investigate the mechanical properties of ultra-thin CSNTs, to compensate for the lack of fundamental study of nanothreads with ultimate configurations.

2. Computational details

2.1. Molecular structures

Many morphologies of DNTs have been synthesized in lab-settings [31–33]. It is well known that carbon nanothreads are highly structure-dependent nanomaterials. Therefore, it is meaningful to investigate the mechanical characteristics of every kind of configuration of nanothreads. Recently, a new experimental finding approved the evidence for CSNTs [5] derived from thiophene, which now extended the synthesis of nanothreads to five-membered aromatic molecules. With its flexibility, it gives the promise to achieve diverse compositions and structures in the future. To obtain meaningful understanding, the detailed information of three molecules was directly borrowed from experimental data of the supporting information (Anti.cif, Syn.cif, and Syn_Anti.cif) in the publication [5], as shown in Fig. 1. Note that, although syn-, anti- and syn-anti thiophene-based CSNTs were proposed, they were not definitively confirmed because it is not currently possible to synthesize pure syn, pure anti and pure syn-anti thiophene-based CSNTs[5]. Based on the nomenclature[34], syn, anti and syn-anti were used to describe sulfurs' position in the CSNTs: nanothreads with sulfur atoms located on only one side, alternating sides, and alternating in pairs, as shown in Fig. 1. To analyze the strain and loading stress during the tensile test, the diameter of all CSNTs was fixed as 0.5 nm, same with the real CSNTs size. The axial length of CSNT Anti, Syn, Syn-anti was set as 0.32 nm, 0.31 nm and 0.28 nm respectively, to achieve clear visualized change during the tensile test. The axial boundary was periodic to effectively avoid the effects of end boundaries and length of single nanothreads on their mechanical properties. Meanwhile, an axial boundary can make the nanothreads infinitely long, even a macrolevel size, to improve the accuracy of the simulation works.

2.2. MD simulations

All MD simulations were realized by applying the Large-scale Atomic/Molecular Massively Parallel Simulator (LAMMPS) package [35]. For the force field, the first-principles-based ReaxFF potential was chosen to perform the MD simulations in the carbon nanothreads. As is known, the first version of ReaxFF was initially developed to mimic dissociation and formation of covalent bonds that are highly computationally demanded for ab initio calculations in carbon-based materials [36]. To date, the ReaxFF was shown to accurately describe a wide range of carbon-based nanostructures because it enables to accurately capture the breaking and formation of covalent bonds due to strain [2,9,37,38]. Moreover, it can perform the interactions of covalent bonds, coulombic forces, and other non-bonded interacting forces, even achieving the values about bond order and bond length, which are important information to capture the change during the tensile process. By using such potential, many studies have successfully proposed specifically structured nanomaterials and evaluated the mechanical properties of diverse carbon-skeleton nanostructures [39–42]. Because our systems of CSNTs are composed of carbon, hydrogen and sulfur atoms, the version of ReaxFF parameterized by Mattsson et al. [43,44] for materials consisting of carbon, hydrogen, oxygen, nitrogen and sulfur atoms, was chosen to predict their mechanical behaviors. This ReaxFF with Mattsson parameter sets has been successfully predicted the mechanical properties of a variety of materials, including crystalline cellulose, composites of a cellulose-carbon nanotube, graphene, functionalized graphene nanoribbons with NH_2, CH_3, OH and C_5H_6 groups and epoxy materials[45–48].

In all MD simulations, the timestep was set as 0.1 fs. At the very beginning, the configuration of each CSNTs model was taken with a minimum energy optimization by an energy tolerance (1.0×10-4 kcal/mol) and a force tolerance (1.0×10^{-4} kcal/mol·Å). The following equilibrium state was obtained after 2 ns, by relaxing without pressure along the axial direction. To prove that the structures are stable after MD simulation time of 2 ns, the potential energy of systems and bond order of the carbon atom in three structures were also calculated, as shown in Figs. S1–2. All those results indicate that the CSNT structures are thermodynamically

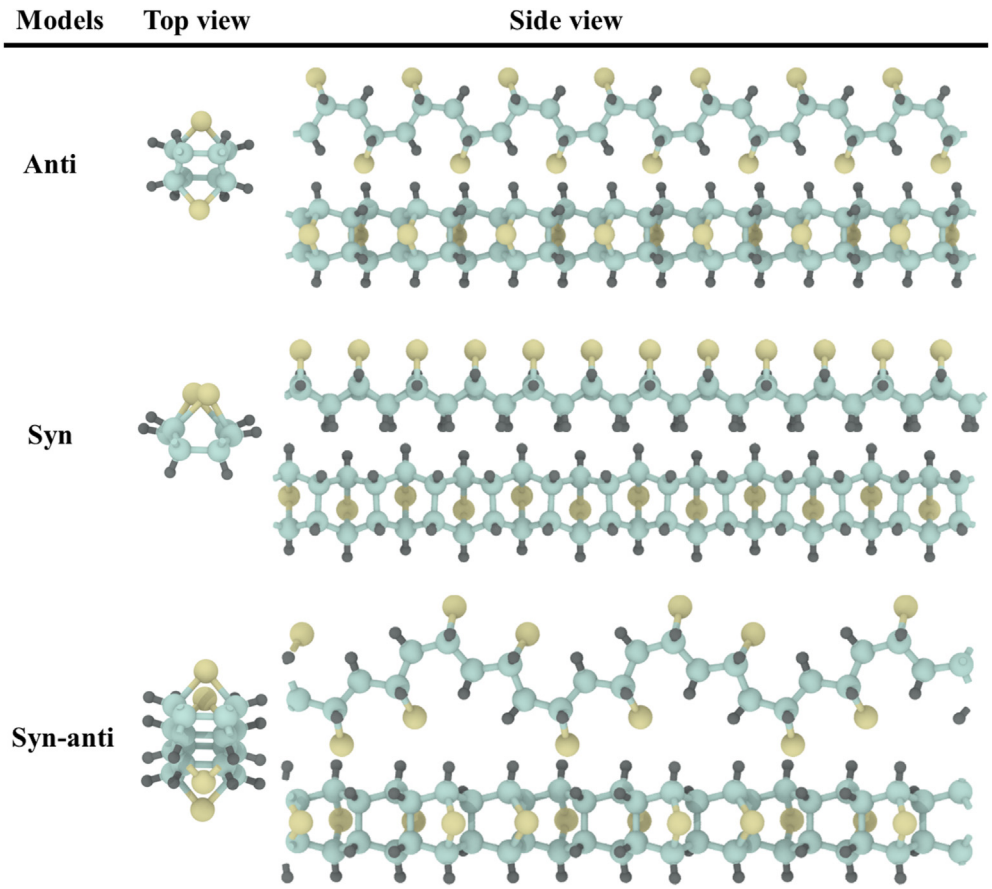

Fig. 1. The top-view and side-view snapshots of molecular configurations of three CSNTs (Anti, Syn, and Syn-anti). The colors, light yellow, powder blue, and dark slate gray sphere indicate sulfur, carbon, and the hydrogen atom, respectively. (A colour version of this figure can be viewed online.)

stable configurations. The NPT ensemble was chosen to use in the MD relaxations. The Nosé-Hoover thermostat and Nosé-Hoover barostat with parameters of damping timestep of 100 and 1000 were utilized, respectively. The deformation along the axial direction was applied with a strain rate of 1.0×10^8 s^{-1} per every 1000 timesteps. And the NVT ensemble was chosen to use in the MD deformation. The real-time value of stress, bond order, and bond length was computed and recorded. In this work, ReaxFF uses distance-dependent bond-order functions to represent the contributions of chemical bonding to the potential energy[38,49,50]. The bond order of specific atoms was computed by the ReaxFF potential specified by pair_style reax/c in LAMMPS. Collecting the global stress of the nanothread is a sufficient way to sum the stress of all atoms. The Young's moduli (E) were calculated from the slope of the fitting of initial strain-stress curves of tensile results.

3. Results and discussion

3.1. Morphology dependent properties

3.1.1. Tensile characteristics of CSNTs

It is known that the mechanical properties of nanomaterials are strongly morphology-dependent. To investigate the effects of all morphologies on the mechanical properties of CSNTs, an ultra-low temperature of 1 K was applied to the tensile tests. The setting of low temperature aims to eliminate most of the influence of thermal kinetics. The real-time engineering strain and stress were calculated, and all stress-strain curves were collected in Fig. 2a. Globally, the results can be roughly described that the relationships between strain and stress are highly nonlinear. The distinct differences between them suggest that the mechanical properties of CSNTs are molecular morphology dependent. The global loading process can be clearly described in several main stages. Following the beginning of the tensile loading, all CSNTs present the first linear elastic response with different elastic strain ranges (Anti, 0–18.7%; Syn, 0–13.6%; Syn-anti, 0–16.4%.). As the loading continues, the stress suddenly drops and then fluctuates slightly around a constant value, forming a swath-like pattern which can be called the yielding stage. Interestingly, Anti and Syn-anti experienced a wide yield strain range. The reason for such unusual mechanical behavior has been explored to be related to the structural transformation of bond configurations of C–C covalent bonds and C–C–C bond angles [51,52], as well as unique molecular morphology. For example, syn-CSNT is a linear molecule and shows identical bond configurations in a one-unit cell along the molecular axis. As a result, subjected to axial tension, syn-CSNT is homogenously deformed, resulting in its almost linear elastic responses followed by brittle fracture. However, for both anti- and syn-anti-CSNTs, they are curved molecules with differently local bond configurations in the one-unit cell along the axial direction. As a consequence, both CSNTs show strong nonlinearity in the tensile stress-strain curves. This is because, as the CSNTs are critically strained, local bond configurations are non-homogenously deformed, resulting in strong nonlinear changes in bond order, bond length and bond angle. To explore whether the plateau features in the stress-strain curves are influenced by straining rate, we performed two more tensile tests of Anti and Syn-anti with strain rates of 1.0×10^8 s^{-1} to 1.0×10^7 s^{-1} for comparison. Fig. S3 shows the tensile stress-strain curves of Anti

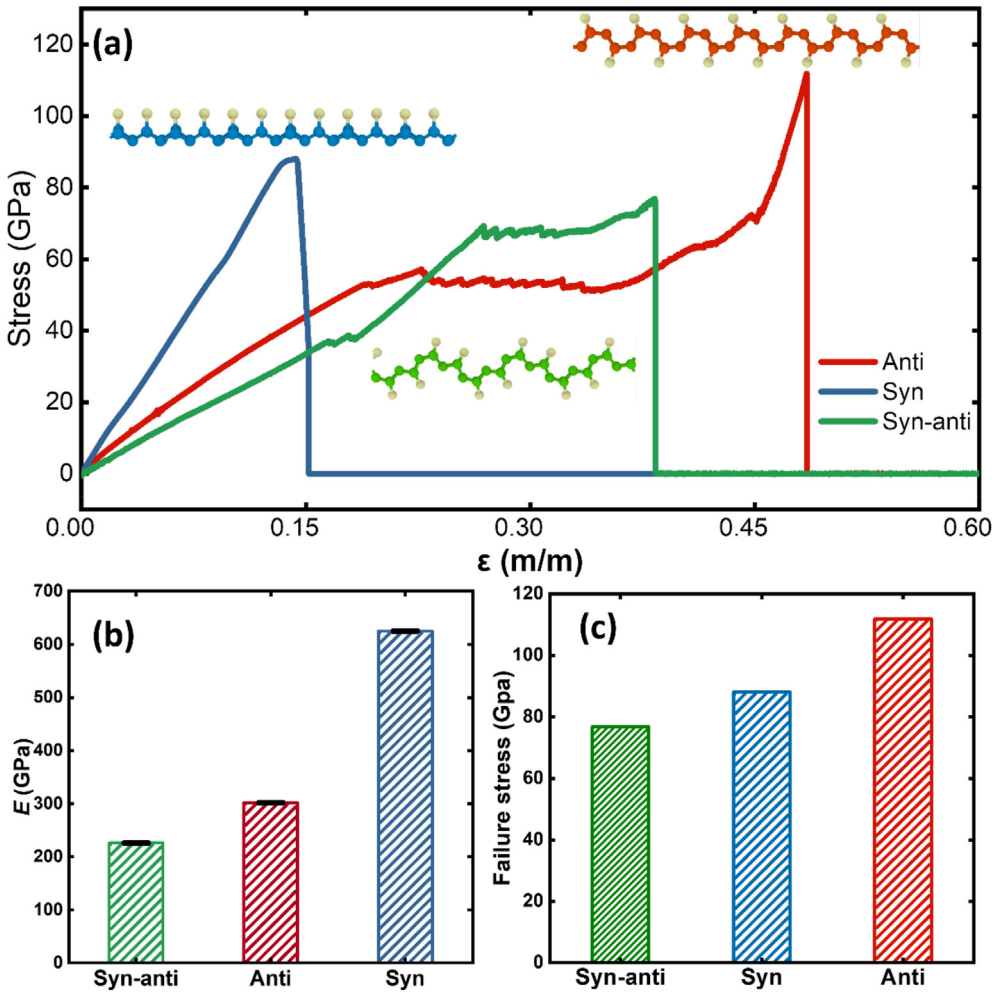

Fig. 2. Tensile results of all CSNTs at temperature 1 K. (a) Tensile stress-strain curves of Anti, Syn and Syn-anti, (b) Young's moduli, and (c) Failure stress. (A colour version of this figure can be viewed online.)

and Syn-anti structures predicted with straining rates of 1.0×10^8 s^{-1}, 2.0×10^7 s^{-1} and 1.0×10^7 s^{-1}. As is indicated, the three tensile stress-strain curves are almost overlapping during the whole straining process, indicating that there is negligible effect of straining rate on the global tensile responses. Therefore, it can be summarized that the plateau features presented in Fig. 2a are negligibly sensitive to the strain rate in the range chosen in this work. Remarkably, before threshold value or rupture stress, all mechanical behaviors are non-linear elastic, not strictly obeying Hooke's law. The stress increases sharply until the threshold value with the loading. Finally, C–C covalent bond breaking results in a drop of stress to zero. Differently from Anti and Syn-anti, Syn's strain-stress curve is in a smooth shape due to its simple morphology. It is worthy to note that all broken bonds resulted from the loading are C–C bonds, not C–S bonds so that mechanical properties of all CSNTs depend mainly on the morphology of their carbon skeletons. More detailed information is shown and discussed in the following section.

In the assumption that the strain range of 0–1% is linear elastic deformation and the area of the cross-section of CSNTs is constant, the axial tensile Young's moduli are calculated by the slope of the stress-strain curve. Herein, Fig. 2b shows the elastic moduli of all studied CSNTs. Similar to the previous studies on CNTs [10,26–28,53] and CNNTs [9], CSNTs also exhibit high Young's modulus (Syn-anti, 226 GPa; Anti, 302 GPa; Syn, 625 GPa). Following the order from the lowest to the highest value, they are sorted as Syn > Anti > Syn-anti. The reason for the distinct discrepancy of tensile stiffness is resulted from different local atom arrangements of CSNTs. Based on Fig. 2a, it is obvious that only carbon atom occurs in the skeleton. Although the sulfur atoms do not affect the tensile properties of CSNTs, their occurrence has an influence on the other carbon atoms' arrangement. There is no bond breaking observed in C–S bonds in all investigated in tensile results. Meanwhile, they all have two effective covalent C–C bonds in the tensile loading cross-sections. Notably, there are always two C–C bonds including in the tensile cross-sections of all CSNTs. The main distinct difference between them is bond angles, resulting in ways of configuration folds. In terms of C–C bond angles, they are ranked as Syn-anti > Anti > Syn. The highest modulus of Syn is attributed to its small bond angles and the simple periodic unit, which make it stronger than others. In comparison, the lowest modulus of Syn-anti is because of its large bond angles and flexible spring-like configurations, which makes it softer and easier to be stretched than others. Similarly, Anti exhibits a smaller modulus than Syn.

The tensile failure stress of all studied CSNTs is collected in Fig. 2c. It also shows a molecule-dependent result, similar to previous studies of CSNTs [9] and CNTs [10]. Following the order from the highest to the lowest value, they are sorted as: Anti (111 GPa) > Syn (88 GPa) > Syn-anti (76 GPa). Commonly, the

tensile strength of nanomaterials is highly relevant to the number of effective cross-sectional covalent bonds. Except for the sulfur atoms, the carbon skeletons of all CSNTs are completely the same and show two effective C–C bonds in the cross-section, when they are stretched to the utmost limit of their ductility. The differences between them are related to the S-doped branch of CSNTs. For the structure of syn and syn-anti, the sulfur atoms are uniquely arranged on one side, resulting in the electrons distribution of two bonded carbon atoms deviating from the axial wire of C–C bonds, thereby weakening C–C covalent bonds. For the structure of anti, however, the location of sulfur atoms has negligible impact on electrons distribution of C–C covalent bonds due to their homogeneous arrangement in the molecule, thereby producing high tensile strength. On the view of 3-dimensional space, sulfur atoms in Anti are distributed more evenly than the others. Such kind of configuration forms the homogeneous interactions between atoms, bonds, and angles on the spatial view, resulting in that there is no apparent localized stress concentration. Therefore, it is the same strength in anywhere of Anti, and the failure stress is likely to perform a global property. In comparison, Syn-anti does not have such equal interaction in its molecular structure. It exhibits weak interactions between the bonds of two periodic units of Syn-anti, where are easier to break than other bonds. Therefore, it is mechanically softer than others due to the non-homogeneous stress-load bond configuration. For the same reason, Syn is the second stiffest CSNT. The detailed information about bonds breaking will be discussed in the following section. It should be noted that all results are investigated under a temperature of 1 K, which means that the effect of thermal kinetics was mostly eliminated. If the temperature is taken into consideration, the value of Young's modulus and failure stress of all CSNTs is different from each other. More information will be shown in the following section.

3.1.2. Bond orders during the tensile tests

Bond orders (BOs) are the key parameter for an atom to evaluate the state of its surrounding bonding, which are highly relevant to bond breaking during tensile deformations. To achieve the detailed information of the BOs, the real-time variation in the atomic BOs following with the axial extension of all CSNTs is considered. Fig. 3 shows the total BOs of one carbon atom located at the end of the breaking bond caused by tensile straining, where they are red-highlighted. Before loading, the value of BOs in all selected carbon atoms is about 3.8, similar to the previous study [10]. It means that the hybridization style of carbon atoms in all CSNTs is sp^3-bonding, rather than sp^2-bonding in graphene or CNTs[5]. For a single carbon atom, it is in a typical motif surrounded by neighboring atoms. As shown in Fig. 3, the total BOs-strain curves of the selected carbon atom are strong non-linearity with variations. Those tendencies can be briefly summarized as that the total BOs are slowly decreasing with the straining before the bond breaking, then suddenly drop. Concretely, every CSNT undergoes various bond, angular and torsional deformations, reflected on the different evolutions of the total BOs during the loading process, which is corresponding to sudden variations in the strain-BOs curves. Before the failure, Anti shows several sudden drops of BOs with increasing strain, while there is a slow reduction of BOs in the elongation of Syn. There are two obvious up-down variations during the elongation of Syn-anti. Notedly, as the strain reached the failure, Syn shows a rapid increase of BOs, then holds around most same stress before the failure. The increase of BO before failure in Fig. 3a is because that there is the stepwise structural transformation of bond configuration that is explained in Fig. S4. Their perfect morphological symmetry leads to highly symmetrical mechanical properties, which makes two C–C bonds located on the failure position of CSNTs simultaneously broken, differing to the helical bond-breaking order of CNNTs [9]. After failure, the rest of the broken CSNTs recover their initial BOs.

Fig. 4 presents the snapshots of Anti at different strains as well as the stress-strain curves under a temperature of 1 K. Anti shows classical brittle fracture characteristics at ultra-low temperature 1 K. The colors of atoms are dependent on the value of their inherent BOs. Apparently, a linear stress-strain relationship appeared as an elastic regime in the strain range of 0.0–0.2, with a slight change of the colors. The nearly same color of all carbon atoms of Anti proves their similar BOs and excellent symmetry of such kind of configuration. Intriguingly, increasing the strain makes no increase of stress on the strain range of 0.23–0.35. The change of color or BOs value on the carbon atoms is not obvious. This can be attributed to the homogeneous extension and deformation of angles & dihedrals of Anti. So, there is only stretching and no mechanical strengthening response. In the same strain range, Fig. 3a also shows a flat curve with no change in the value of BOs. Here, the snapshots exhibit that the carbon atoms bonding with sulfur atoms show lower BOs than ones only bonding with carbon atoms or hydrogen atoms. Even so, the brittle fracture occurs among carbon atoms, when the stress reaches the failure value. At the strain of 0.49, two C–C covalent bonds are broken simultaneously into two independent parts in the initial configuration of Anti. For comparison, the snapshots of Syn and Syn-anti at different strains also are shown in Fig. S5 and Fig. S6.

3.2. The role of temperature

3.2.1. Tensile performance of CSNTS

The thermal effect plays an important role in the mechanical performance of CSNTs. In this study, a wide range of temperatures have been considered. Aiming at understanding the thermal influence on the tensile properties of CSNTs, the evaluations of stress-strain curves at various temperatures are investigated and collected in Fig. 5. The mechanical properties of CSNTs vary at various temperatures. A temperature range of 1–1500 K is used for Anti's tensile tests, while the temperature range of 1–1200 K and 1–700 K are used for Syn and Syn-anti due to their thermal instability at high temperatures. It is found that CSNTs exhibit an excellent and stable mechanical property under elevated temperatures. In the strain range up to 0.0–1.0%, Young's moduli of CSNTs are calculated, as shown in Fig. 6. Generally, it is not a linear relationship between elasticity and temperatures. Various temperatures lead to a slight changing of Young's moduli of CSNTs except for the one of Syn at a temperature of 500 K. The elasticity of CSNTs at the beginning of elongation is quite stable and nearly independent of the temperature. Furthermore, all of them exhibit outstanding elasticity that Anti, Syn, and Syn-anti possess Young's modulus around 300 GPa, 500 GPa, and 250 GPa, respectively. As is known, there is apparent temperature-induced softening in the mechanical stiffness of conventional materials. For carbon-based nanothreads, previous studies revealed that there is no monotonic trend in Young's moduli with temperature [9,22,26,54], however, the temperature has a large influence on the failure strength and strain. For our CSNTs, we found that tensile Young's modulus non-monotonically varies with temperature. Similar to carbon nanothreads, there is shortening and lengthening of the skeleton of CSNTs with increasing temperature and the percentage of bond shortening/lengthening is changeable with temperature, thereby resulting in the non-monotonic change in Young's modulus with temperature. Based on their lightweight and high elasticity, CSNTs are expected to be a potential candidate for high-density mechanical energy storage materials [55].

Furthermore, the variation of failure stress and rupture strain at all temperatures are collected from Fig. 5 into Fig. 7a and Fig. 7b.

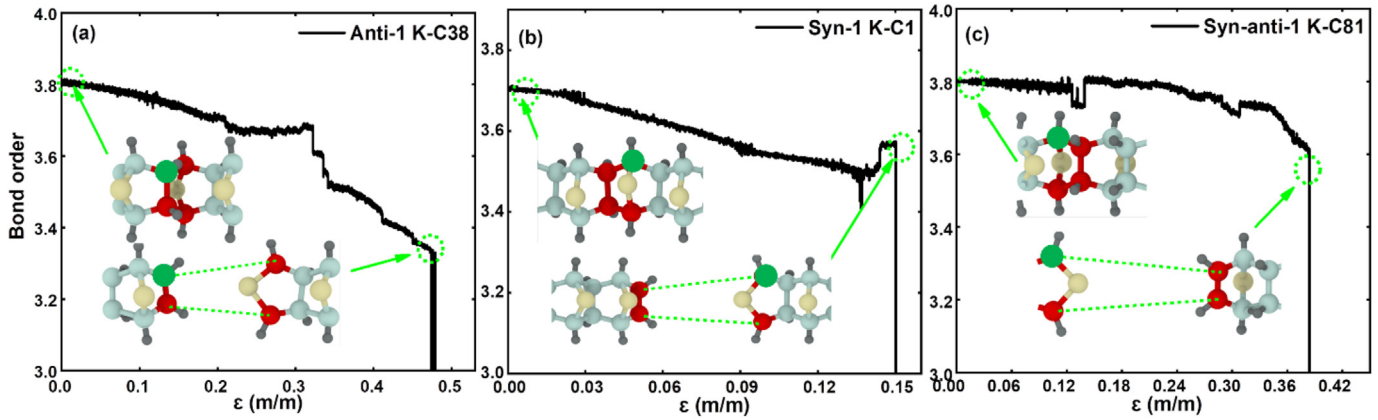

Fig. 3. The changes of the bond order of the carbon atom in CSNTs resulted from mechanical elongation at temperature 1 K. The red-color atoms are the carbon atoms participating in the bond breaking, the green-color atoms are analyzed by calculating it BO. The other colors light yellow, powder blue, and dark slate gray sphere indicate sulfur, carbon, and the hydrogen atom, respectively. (A colour version of this figure can be viewed online.)

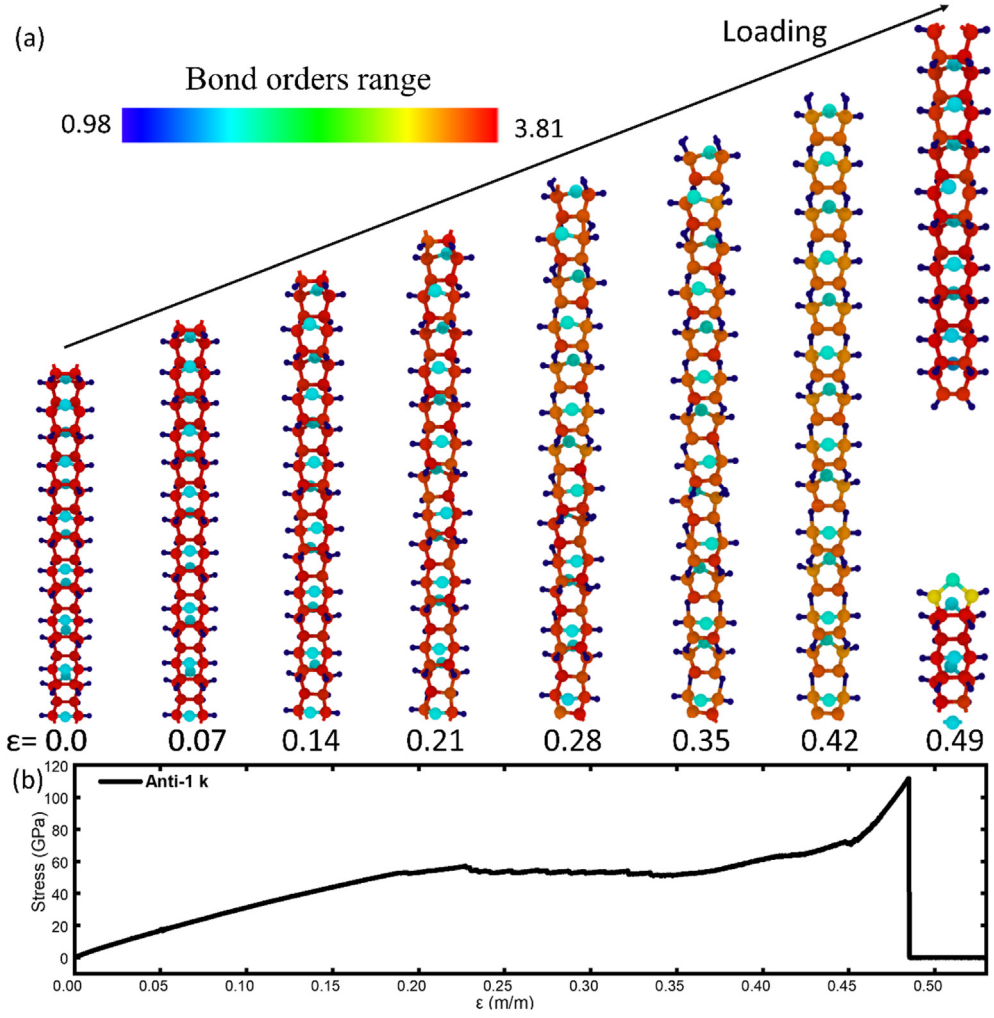

Fig. 4. The strain-stress curve of Anti at temperature 1 K, and the snapshots of morphology at different strains. The colors of atoms are depended on the value of their bond orders. (A colour version of this figure can be viewed online.)

The failure stress-temperature curves in Fig. 7a indicate that temperature affects distinctly the failure stress. Differing from elasticity performance, failure stress reduces with elevated temperature. Although Anti is robust with the maximum failure stress value of 111 GPa at an extreme-low temperature of 1 K, it becomes weaker when the temperature increases from 100 K to 1000 K. With the increase of temperature, the failure stress reduces slowly, until a sudden decrease at ultra-high temperature. In terms of rupture

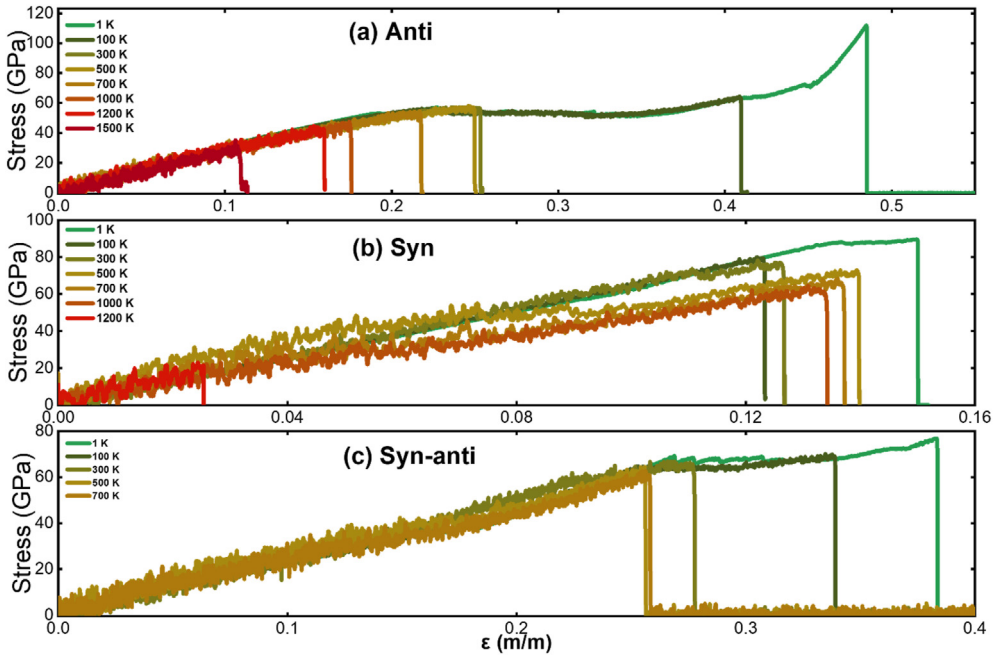

Fig. 5. Tensile results of CSNTs under different temperatures. (a)–(c) strain-stress curves of Anti, Syn, and Syn-anti. (A colour version of this figure can be viewed online.)

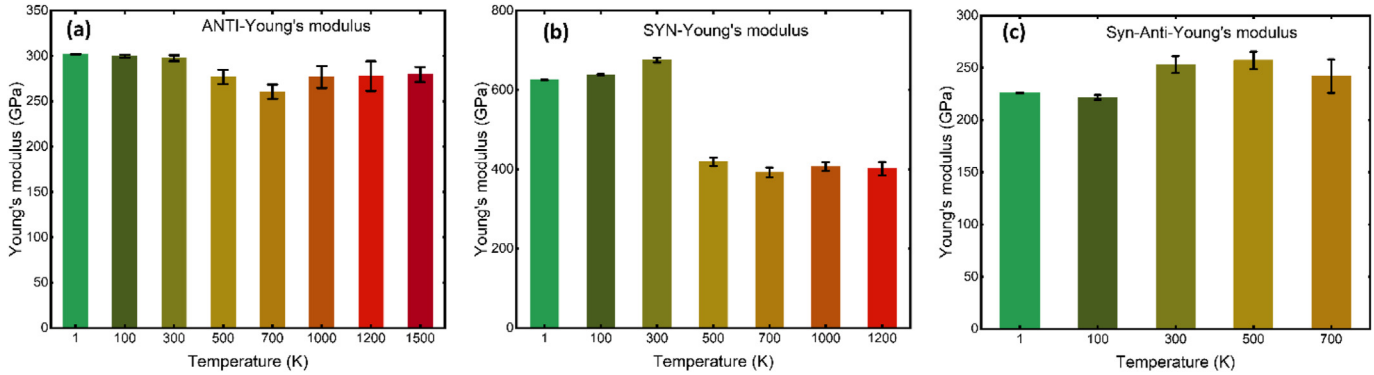

Fig. 6. Young's moduli of the carbon sulfur nanothreads at different temperatures. (a) Anti, (b) Syn, and (c) Syn-Anti. (A colour version of this figure can be viewed online.)

strain in Fig. 7b, both Anti and Syn-anti become easier to be fractured when the temperature increases. However, Syn shows a slight increase in Young's modulus with the increase of temperature from 100 to 1000 K. Comparing with failure stress and rupture strain, the stiffnesses of CSNTs are rarely dependent on the temperature, which is analogous with DNTs [10,26] and CNNTs [9].

3.2.2. *The effect of temperature on the BOs and bond length in CSNTS*

To explore the local chemical bond change of CSNTs during increasing temperature, the variation in the BOs and bond length with axial elongation under different temperatures are recorded. Fig. 8 shows the BOs-strain curves of the local carbon atom where bond-breaking happens in the robust Anti under temperature from 1 to 1500 K. The BO value highly fluctuates with elevated temperature, corresponding with stress-strain curves of Anti. Unlike DNTs [10,26] and CNNTs [9], the BOs of Anti show a relatively flat regime before fracturing of the bond, then sharp drops at the fracture, at all temperatures except for 1, 100 and 500 K. It implies that the local carbon atom at the end of the fractured bond is always in a quite stable state before the fracture. This phenomenon is also verified by the bond length change caused by the elongation. Fig. 9 plots the relationships of bond length-strain of local fracture bond in robust Anti at mechanical failure under temperature varying from 1 to 1500 K. The bond length curves of Anti indicate that the C–C bonds in the skeleton are nonlinearly changed before mechanical fracture, and it increases sharply at the failure. Based on the observation of BOs and bond length, it shows that changes in BOs of local carbon atom and bong length of C–C bond in Anti before failure stress are insignificant compared with its global elongation strain. This suggests that the stretching of local bond angles and dihedral angles devotes the key contribution to the global mechanical elongation, unlike DNTs and CNNTs in which their axial elongations are mainly caused by angle, dihedral, and torsional deformations. The failure stress of CSNTs depends on the strength of the C–C covalent bond in their mechanical skeleton. In addition, Syn and Syn-anti also exhibit similar mechanical performance with Anti, as the results show in the supporting information (From Fig. S7 to Fig. S10).

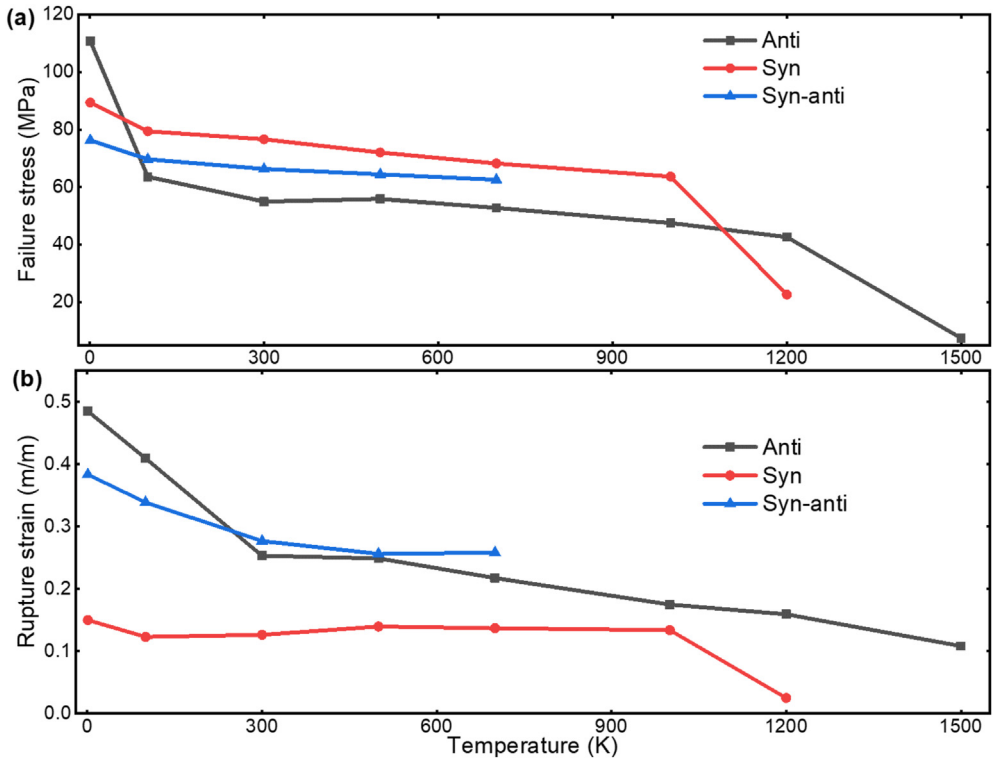

Fig. 7. (a)Failure stress and (b)rupture strain varied with different temperatures. (A colour version of this figure can be viewed online.)

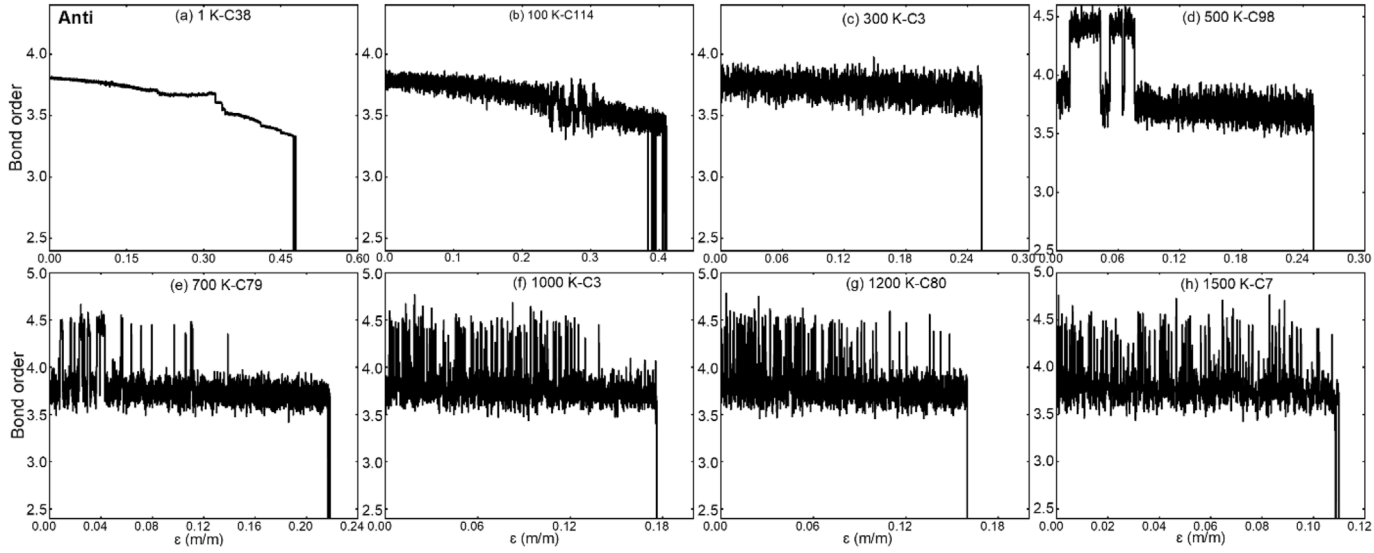

Fig. 8. Variation in the BOs of one carbon atom of Anti CSNT with axial strain at temperatures varying from 1 to 1500 K.

4. Conclusions

In summary, we investigated the tensile mechanical characteristics of syn-, anti- and syn-anti thiophene-based CSNTs by applying MD simulations with a first-principles-based ReaxFF forcefield. This work puts emphasis on the effect of morphology and temperature on the tensile mechanical properties. Similar to conventional DNTs, the tensile properties of CSNTs are dependent on both morphology and temperature. CSNTs exhibit outstanding mechanical properties including high tensile Young's modulus (221–681 GPa), strong axial tensile strength (up to 110 GPa), and excellent ductility (up to 50%). As the ultra-thin carbon nanothreads, CSNTs show different tensile mechanisms, differing from the previously studied carbon nanothreads. The results reveal that there are slight changes in BOs and bond length in CSNTs with loading elongation before failure. The stretching of the bond angles and dihedral angles in the main skeleton contributes to the main part of the global tensile strain. Due to the highly global symmetry of configuration, simultaneous bond-breaking happens in the carbon skeleton of CSNTs. But this deformation doesn't include torsional deformation. The upper limit of the strength of CSNTs primarily relies on the strength of C–C covalent bonds located on

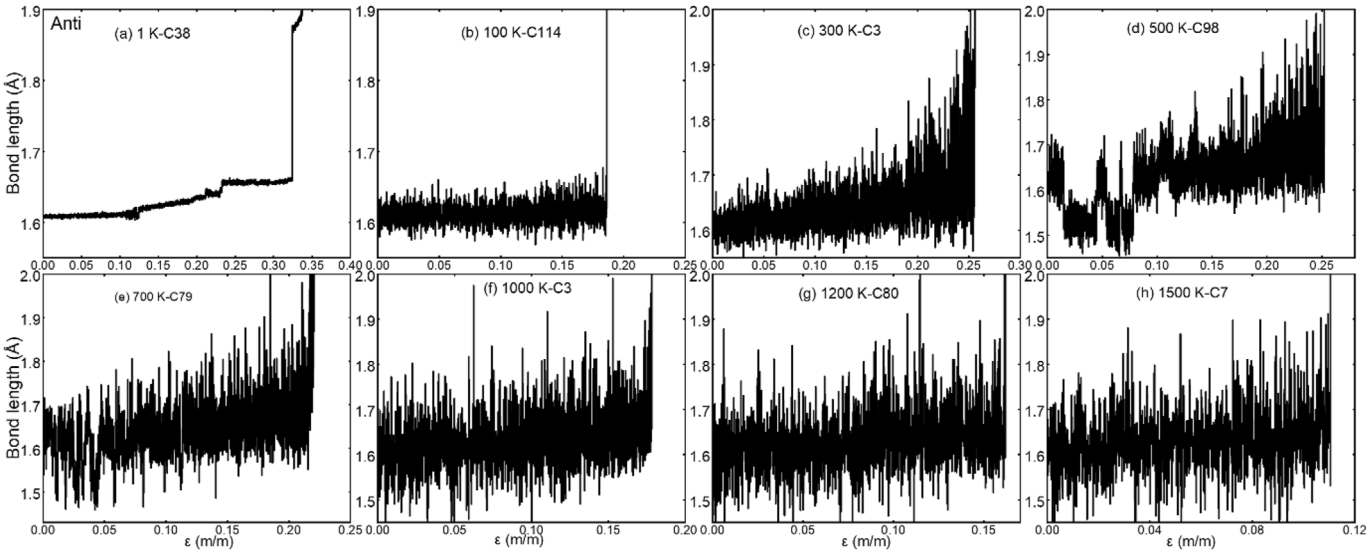

Fig. 9. Variation in a localized bond length with globally axial strain for Anti CSNT at temperatures ranging from 1 to 1500 K.

the carbon skeleton. With a superior lightweight, global symmetry and outperforming mechanical properties, CSNTs are expected to be a potential material candidate related to symmetry-dependent piezoelectricity or of high-density mechanical energy storage.

CRediT authorship contribution statement

Yuequn Fu: Conceptualization, Methodology, Visualization, Software, Writing – original draft. **Jianyang Wu:** Data curation, Writing – original draft, Writing – review & editing. **Senbo Xiao:** Investigation, Writing – review & editing. **Siqi Liu:** Writing – review & editing. **Zhiliang Zhang:** Supervision, Writing – review & editing. **Jianying He:** Supervision, Writing – review & editing.

Declaration of competing interest

The authors declare that they have no known competing financial interests or personal relationships that could have appeared to influence the work reported in this paper.

Acknowledgments

This work is financially supported by the Research Council of Norway (Grant No. 234626), the China Scholarship Council, the National Natural Science Foundation of China (Grant Nos. 11772278 and 11502221), the Jiangxi Provincial Outstanding Young Talents Program (Grant No. 20192BCBL23029), the Fundamental Research Funds for the Central Universities (Xiamen University: Grant No. 20720180014). The supercomputer CPU hours were provided by the Norwegian Metacenter for Computational science (Project ID: NN9110K and NN9391K).

Appendix A. Supplementary data

Supplementary data to this article can be found online at https://doi.org/10.1016/j.carbon.2021.08.006.

References

[1] L. Ciabini, M. Santoro, F.A. Gorelli, R. Bini, V. Schettino, S. Raugei, Triggering dynamics of the high-pressure benzene amorphization, Nat. Mater. 6 (1) (2007) 39–43.
[2] R.E. Roman, K. Kwan, S.W. Cranford, Mechanical properties and defect sensitivity of diamond nanothreads, Nano Lett. 15 (3) (2015) 1585–1590.
[3] H.-T. Huang, L. Zhu, M.D. Ward, T. Wang, B. Chen, B.L. Chaloux, et al., Nanoarchitecture through Strained molecules: cubane-derived scaffolds and the smallest carbon nanothreads, J. Am. Chem. Soc. 142 (42) (2020) 17944–17955.
[4] T.C. Fitzgibbons, M. Guthrie, E-s Xu, V.H. Crespi, S.K. Davidowski, G.D. Cody, et al., Benzene-derived carbon nanothreads, Nat. Mater. 14 (1) (2015) 43–47.
[5] A. Biswas, M.D. Ward, T. Wang, L. Zhu, H.-T. Huang, J.V. Badding, et al., Evidence for orientational order in nanothreads derived from thiophene, J. Phys. Chem. Lett. 10 (22) (2019) 7164–7171.
[6] D.J. McClements, S.M. Jafari, Improving emulsion formation, stability and performance using mixed emulsifiers: a review, Adv. Colloid Interface Sci. 251 (2018) 55–79.
[7] A. Shinozaki, K. Mimura, T. Nishida, T. Inoue, S. Nakano, H. Kagi, Stability and partial oligomerization of naphthalene under high pressure at room temperature, Chem. Phys. Lett. 662 (2016) 263–267.
[8] S.J. Juhl, T. Wang, B. Vermilyea, X. Li, V.H. Crespi, J.V. Badding, et al., Local structure and bonding of carbon nanothreads probed by high-resolution transmission electron microscopy, J. Am. Chem. Soc. 141 (17) (2019) 6937–6945.
[9] Y. Fu, K. Xu, J. Wu, Z. Zhang, J. He, The effects of morphology and temperature on the tensile characteristics of carbon nitride nanothreads, Nanoscale 12 (23) (2020) 12462–12475.
[10] C. Feng, J. Xu, Z. Zhang, J. Wu, Morphology- and dehydrogenation-controlled mechanical properties in diamond nanothreads, Carbon 124 (2017) 9–22.
[11] J. Xue, Y. Xie, Q. Peng, Y. Chen, Thermal transports of one-dimensional ultrathin carbon structures, Nanotechnology 30 (47) (2019) 475401.
[12] P.G. Demingos, A.R. Muniz, Electronic and mechanical properties of partially saturated carbon and carbon nitride nanothreads, J. Phys. Chem. C 123 (6) (2019) 3886–3891.
[13] M.D. Lima, N. Li, M.J. De Andrade, S. Fang, J. Oh, G.M. Spinks, et al., Electrically, chemically, and photonically powered torsional and tensile actuation of hybrid carbon nanotube yarn muscles, Science 338 (6109) (2012) 928–932.
[14] C.S. Haines, N. Li, G.M. Spinks, A.E. Aliev, J. Di, R.H. Baughman, New twist on artificial muscles, Proc. Natl. Acad. Sci. Unit. States Am. 113 (42) (2016) 11709–11716.
[15] J. Di, X. Zhang, Z. Yong, Y. Zhang, D. Li, R. Li, et al., Carbon-nanotube fibers for wearable devices and smart textiles, Adv. Mater. 28 (47) (2016) 10529–10538.
[16] H. Zhan, G. Zhang, J.M. Bell, V.B. Tan, Y. Gu, High density mechanical energy storage with carbon nanothread bundle, Nat. Commun. 11 (1) (2020) 1–11.
[17] K. Duan, Y. Li, L. Li, Y. Hu, X. Wang, Diamond nanothread based resonators: ultrahigh sensitivity and low dissipation, Nanoscale 10 (17) (2018) 8058–8065.
[18] T. Zhu, E. Ertekin, Phonons, localization, and thermal conductivity of diamond nanothreads and amorphous graphene, Nano Lett. 16 (8) (2016) 4763–4772.
[19] X. Li, M. Baldini, T. Wang, B. Chen, E-s Xu, B. Vermilyea, et al., Mechanochemical synthesis of carbon nanothread single crystals, J. Am. Chem. Soc. 139 (45) (2017) 16343–16349.
[20] W. Li, C. Jayasinghe, V. Shanov, M. Schulz, Spinning carbon nanotube nanothread under a scanning electron microscope, Materials 4 (9) (2011) 1519–1527.
[21] H.-T. Huang, L. Zhu, M.D. Ward, T. Wang, B. Chen, B.L. Chaloux, et al., Nanoarchitecture through strained molecules: cubane-derived scaffolds and the

smallest carbon nanothreads, J. Am. Chem. Soc. 142 (42) (2020) 17944–17955.
[22] J.F. Silveira, A.R. Muniz, First-principles calculation of the mechanical properties of diamond nanothreads, Carbon 113 (2017) 260–265.
[23] J. Xiao, M.-M. Chen, W.-J. Liu, J. He, C.-N. Pan, M.-Q. Long, Perfect mechanical and robust electronic properties of new carbon nanothreads: a first principles study, Phys. E Low-dimens. Syst. Nanostruct. 111 (2019) 37–43.
[24] P.G. Demingos, A.R. Muniz, Carbon nanothreads from polycyclic aromatic hydrocarbon molecules, Carbon 140 (2018) 644–652.
[25] L.W. Zhang, W.M. Ji, K.M. Liew, Mechanical properties of diamond nanothread reinforced polymer composites, Carbon 132 (2018) 232–240.
[26] H. Zhan, G. Zhang, V.B. Tan, Y. Cheng, J.M. Bell, Y.W. Zhang, et al., From brittle to ductile: a structure dependent ductility of diamond nanothread, Nanoscale 8 (21) (2016) 11177–11184.
[27] J.F. Silveira, A.R. Muniz, Functionalized diamond nanothreads from benzene derivatives, Phys. Chem. Chem. Phys. 19 (10) (2017) 7132–7137.
[28] R.E. Roman, K. Kwan, S.W. Cranford, Mechanical properties and defect sensitivity of diamond nanothreads, Nano Lett. 15 (3) (2015) 1585–1590.
[29] L.A. Openov, A.I. Podlivaev, Thermal stability of diamond-like carbon nanothreads, JETP Lett. (Engl. Transl.) 104 (3) (2016) 193–196.
[30] S. Huss, S. Wu, B. Chen, T. Wang, M.C. Gerthoffer, D.J. Ryan, et al., Scalable synthesis of crystalline one-dimensional carbon nanothreads through modest-pressure polymerization of furan, ACS Nano 15 (3) (2021) 4134–4143.
[31] E.S. Xu, P.E. Lammert, V.H. Crespi, Systematic enumeration of sp(3) nanothreads, Nano Lett. 15 (8) (2015) 5124–5130.
[32] T.C. Fitzgibbons, M. Guthrie, E.S. Xu, V.H. Crespi, S.K. Davidowski, G.D. Cody, et al., Benzene-derived carbon nanothreads, Nat. Mater. 14 (1) (2015) 43–47.
[33] T. Wang, P. Duan, E.-S. Xu, B. Vermilyea, B. Chen, X. Li, et al., Constraining carbon nanothread structures by experimental and calculated nuclear magnetic resonance spectra, Nano Lett. 18 (8) (2018) 4934–4942.
[34] B. Chen, R. Hoffmann, N. Ashcroft, J. Badding, E. Xu, V. Crespi, Linearly polymerized benzene arrays as intermediates, tracing pathways to carbon nanothreads, J. Am. Chem. Soc. 137 (45) (2015) 14373–14386.
[35] Plimpton S, Hendrickson B. Parallel molecular dynamics algorithms for simulation of molecular systems. ACS (Am. Chem. Soc.) Symp. Ser.: Citeseer; p. 114-114.
[36] A.C. Van Duin, S. Dasgupta, F. Lorant, W.A. Goddard, ReaxFF: a reactive force field for hydrocarbons, J. Phys. Chem., A 105 (41) (2001) 9396–9409.
[37] H. Zhan, G. Zhang, J.M. Bell, Y. Gu, The morphology and temperature dependent tensile properties of diamond nanothreads, Carbon 107 (2016) 304–309.
[38] K. Chenoweth, A.C. Van Duin, W.A. Goddard, ReaxFF reactive force field for molecular dynamics simulations of hydrocarbon oxidation, J. Phys. Chem., A 112 (5) (2008) 1040–1053.
[39] T.P. Senftle, S. Hong, M.M. Islam, S.B. Kylasa, Y. Zheng, Y.K. Shin, et al., The ReaxFF reactive force-field: development, applications and future directions, NPJ Comput. Mater. 2 (1) (2016).
[40] H. Zhao, Q. Shi, Z. Han, H. Gong, Z. Zhang, S. Wu, et al., Anomalous thermal stability in supergiant onion-like carbon fullerenes, Carbon 138 (2018) 243–256.
[41] C. Sui, Y. Zhao, Z. Zhang, J. He, Z. Zhang, X. He, et al., Morphology-Controlled tensile mechanical characteristics in graphene allotropes, ACS Omega 2 (7) (2017) 3977–3988.
[42] J.M. de Sousa, T. Botari, E. Perim, R.A. Bizao, D.S. Galvao, Mechanical and structural properties of graphene-like carbon nitride sheets, RSC Adv. 6 (80) (2016) 76915–76921.
[43] T.R. Mattsson, J.M.D. Lane, K.R. Cochrane, M.P. Desjarlais, A.P. Thompson, F. Pierce, et al., First-principles and classical molecular dynamics simulation of shocked polymers, Phys. Rev. B 81 (5) (2010), 054103.
[44] T. Mattsson, J. Lane, K. Cochrane, M. Desjarlais, A. Thompson, F. Pierce, et al., Reactive MD-force field: general-purpose hydrocarbon parameterization, Phys. Rev. B 81 (2010), 054103.
[45] E. Zaminpayma, P. Nayebi, Mechanical and electrical properties of functionalized graphene nanoribbon: a study of reactive molecular dynamic simulation and density functional tight-binding theory, Phys. B Condens. Matter 459 (2015) 29–35.
[46] X. Wu, R.J. Moon, A. Martini, Tensile strength of I β crystalline cellulose predicted by molecular dynamics simulation, Cellulose 21 (4) (2014) 2233–2245.
[47] X. Wu, R.J. Moon, A. Martini, Crystalline cellulose elastic modulus predicted by atomistic models of uniform deformation and nanoscale indentation, Cellulose 20 (1) (2013) 43–55.
[48] Y. Li, H. Zhu, Y. Wang, U. Ray, S. Zhu, J. Dai, et al., Cellulose-nanofiber-Enabled 3D printing of a carbon-nanotube microfiber network, Small Methods 1 (10) (2017) 1700222.
[49] H.M. Aktulga, J.C. Fogarty, S.A. Pandit, A.Y. Grama, Parallel reactive molecular dynamics: numerical methods and algorithmic techniques, Parallel Comput. 38 (4–5) (2012) 245–259.
[50] L. Liu, Y. Liu, S.V. Zybin, H. Sun, W.A. Goddard III, ReaxFF-lg: correction of the ReaxFF reactive force field for London dispersion, with applications to the equations of state for energetic materials, J. Phys. Chem., A 115 (40) (2011) 11016–11022.
[51] J. Wu, J. He, G.M. Odegard, S. Nagao, Q. Zheng, Z. Zhang, Giant stretchability and reversibility of tightly wound helical carbon nanotubes, J. Am. Chem. Soc. 135 (37) (2013) 13775–13785.
[52] X. Chen, S. Zhang, D.A. Dikin, W. Ding, R.S. Ruoff, L. Pan, et al., Mechanics of a carbon nanocoil, Nano Lett. 3 (9) (2003) 1299–1304.
[53] J.F.R.V. Silveira, A.R. Muniz, First-principles calculation of the mechanical properties of diamond nanothreads, Carbon 113 (2017) 260–265.
[54] Z. Zheng, H. Zhan, Y. Nie, X. Xu, Y. Gu, Role of nitrogen on the mechanical properties of the novel carbon nitride nanothreads, J. Phys. Chem. C 123 (47) (2019) 28977–28984.
[55] Y. Fu, S. Xiao, S. Liu, J. Wu, X. Wang, L. Qiao, et al., Stability, deformation and rupture of Janus oligomer enabled self-emulsifying water-in-oil microemulsion droplets, Phys. Chem. Chem. Phys. 22 (43) (2020) 24907–24916.